









## Article

# Optimization of Biodiesel Production Process Using MoO<sub>3</sub> Catalysts and Residual Oil: A Comprehensive Experimental 2<sup>3</sup> Study

Adriano Lima da Silva <sup>1,\*</sup>, Helder de Lucena Pereira <sup>1</sup>, Herbet Bezerra Sales <sup>1</sup>, Juliana Kelly Dionizio <sup>1</sup>,  
Mary Cristina Ferreira Alves <sup>2</sup>, Danyelle Garcia Guedes <sup>1</sup>, Carlos Bruno Barreto Luna <sup>3</sup>  
and Ana Cristina Figueiredo de Melo Costa <sup>1</sup>

<sup>1</sup> Synthesis Laboratory of Ceramic Materials (LabSMaC), Graduate Program in Materials Science and Engineering (PPGCEMat), Federal University of Campina Grande (UFCG), Campina Grande 58429-900, Brazil; hld.lucena@gmail.com (H.d.L.P.); herbet\_bezerra@hotmail.com (H.B.S.); julianakelly71@gmail.com (J.K.D.); danyelle.garcia@estudante.ufcg.edu.br (D.G.G.); ana.figueiredo@professor.ufcg.edu.br (A.C.F.d.M.C.)

<sup>2</sup> Graduate Program in Chemistry (PPGQ), State University of Paraíba (UEPB), Campina Grande 58429-900, Brazil; mary.alves@servidor.uepb.edu.br

<sup>3</sup> Materials Engineering Academic Unit, Polymer Processing Laboratory, Federal University of Campina Grande, Av. Aprígio Veloso, 882, Campina Grande 58429-900, Brazil; brunobarretodemaufcg@hotmail.com

\* Correspondence: adrianolimadasilva@hotmail.com

**Abstract:** The study aimed to utilize MoO<sub>3</sub> catalysts, produced on a pilot scale via combustion reaction, to produce biodiesel from residual oil. Optimization of the process was conducted using a 2<sup>3</sup> experimental design. Structural characterization of the catalysts was performed through X-ray diffraction, fluorescence, Raman spectroscopy, and particle size distribution analyses. At the same time, thermal properties were examined via thermogravimetry and differential thermal analysis. Catalytic performance was assessed following process optimization. α-MoO<sub>3</sub> exhibited a monophasic structure with orthorhombic phase, whereas α/h-MoO<sub>3</sub> showed a biphasic structure. α-MoO<sub>3</sub> had a larger crystallite size and higher crystallinity, with thermal stability observed up to certain temperatures. X-ray fluorescence confirmed molybdenum oxide predominance in the catalysts, with traces of iron oxide. Particle size distribution analyses revealed polymodal distributions attributed to structural differences. Both catalysts demonstrated activity under all conditions tested, with ester conversions ranging from 93% to 99%. The single-phase catalyst had a long life cycle and was reusable for six biodiesel production cycles. The experimental design proved to be predictive and significant, with the type of catalyst being the most influential variable. Optimal conditions included α-MoO<sub>3</sub> catalyst, oil/alcohol ratio of 1/15, and a reaction time of 60 min, resulting in high biodiesel conversion rates and showcasing the viability of MoO<sub>3</sub> catalysts in residual oil biodiesel production.

**Keywords:** planning; factorial; transesterification; esterification; industry



**Citation:** Silva, A.L.d.; Pereira, H.d.L.; Sales, H.B.; Dionizio, J.K.; Alves, M.C.F.; Guedes, D.G.; Luna, C.B.B.; Costa, A.C.F.d.M. Optimization of Biodiesel Production Process Using MoO<sub>3</sub> Catalysts and Residual Oil: A Comprehensive Experimental 2<sup>3</sup> Study. *Molecules* **2024**, *29*, 2404. <https://doi.org/10.3390/molecules29102404>

Academic Editors: Yin Hu and Chaoqun Bian

Received: 26 April 2024

Revised: 14 May 2024

Accepted: 17 May 2024

Published: 20 May 2024



**Copyright:** © 2024 by the authors. Licensee MDPI, Basel, Switzerland. This article is an open access article distributed under the terms and conditions of the Creative Commons Attribution (CC BY) license (<https://creativecommons.org/licenses/by/4.0/>).

## 1. Introduction

Researchers worldwide have directed their efforts to explore alternative energy sources, aiming to mitigate the negative impacts of climate change. Over the past two decades, there has been a significant transition from fossil fuels to adopting more efficient and low-carbon resources in producing sustainable fuels [1,2]. Biodiesel, known as alkyl esters, is obtained through the esterification of fatty acids and the transesterification of triglycerides, including animal or vegetable fat residues. In these processes, the reaction between a lipid and an alcohol, such as ethanol or methanol, occurs in the presence of a catalyst [3].

Biodiesel has several advantages such as its biodegradability, reduced greenhouse gas emissions profile, and lower sulfur and particulate emissions [4]. As for the raw material for

producing this biofuel, waste oil not only makes the process economically viable but also avoids competition with edible oils, providing an environmentally appropriate solution for the disposal of frying oil waste.

A wide range of catalysts are used in biodiesel synthesis [5], covering types such as acid [6], basic [7], homogeneous [8], heterogeneous [9], ionic [10], among others. Solid acid catalysts have advantages such as high conversion of fatty oils into biodiesel, water tolerance, reduced waste treatment costs, and production of purer glycerol. Additionally, they are easily separated, reused, and regenerated as needed, resulting in less leaching from activity sites [11,12]. Catalysts that have molybdenum [13] as the main component have aroused great interest due to their acidic properties, Lewis and Brønsted, and their ability to exist in different oxidation states. These demonstrate promise for applications in industrial catalytic processes [14].

The combustion reaction is considered a relatively simple, effective, and low-cost technique, widely established in the literature as a procedure used for the synthesis of various types of oxides [15–17] with applications in the production of biodiesel [18]. The innovative aspect of this work is in the consolidation of  $\text{MoO}_3$  catalysts obtained through the combustion reaction, offering a significant contribution to studies on the optimization of the biofuel production process.

In addition to the catalyst, factors such as temperature, time, alcohol/oil ratio, amount of catalyst, and type of oil are crucial to improving the effectiveness of esterification and transesterification reactions. Each of these elements presents opportunities for optimization, both in terms of energy and chemical consumption and in relation to the process's environmental impact [19,20]. It is crucial to carefully plan experiments and methods to achieve maximum biodiesel yields with efficient resource utilization. Optimization techniques, including linear and non-linear equations, are highly recommended for this purpose. These techniques are advantageous because they are easy to analyze and capable of resolving complex conditions effectively [21].

Recent studies have focused on optimizing the reaction parameters of biodiesel production by heterogeneous catalysis using different methodologies [22,23] such as supervised regression; Huber regression; LASSO; RVS and RNA models [24]; response surface methodology (RSM) [25–28] metaheuristic algorithms like GA, PSO, and FA [29]; multiparametric optimization [30]; and factorial experimental design [22,24,26,29,31].

Arrais Gonçalves, Karine Lourenço Mares, Roberto Zamian, Narciso da Rocha Filho, and Rafael Vieira da Conceição [32] studied the ideal conditions for biodiesel production using the acidic heterogeneous magnetic catalyst  $\text{MoO}_3/\text{SrFe}_2\text{O}_4$ . The optimal reaction conditions were established as a temperature of 164 °C, alcohol/oil molar ratio of 40:1, catalyst dosage of 10%, and reaction time of 4 h, resulting in an ester conversion of 95.4%. The catalyst showed catalytic and magnetic activity even after eight reaction cycles, suggesting its viability for future applications. de Brito, Gonçalves, dos Santos, da Rocha Filho, and da Conceição [33] used the catalyst of 30- $\text{MoO}_3/\text{Nb}_2\text{O}_5$  in the synthesis of biodiesel by transesterification. Under optimized conditions (145 °C, 2.5 h, 20:1 methanol/oil molar ratio, and 6% catalyst), a 94.2% conversion to esters was achieved.

Zhang and Xie (2023) [13] investigated the performance of a ZrMo catalyst in FFA esterification of simulated acidic oils containing 20 wt% oleic acid. FFA conversion reached 89.3% after 1 h of reaction and increased to 94.7% when the reaction lasted 5 h. Wang et al. (2022) [20] compared transesterification activity with esterification using the  $\text{MoO}_3/\text{ZrO}_2/\text{KIT-6}$  catalyst. The results showed that FFA conversion was significantly higher than oil conversion, suggesting that the catalyst catalyzes FFA esterification more efficiently than oil transesterification. The esterification conversion reached 88.5% in 1 h and increased to 96.7% in 6 h.

Based on the studies referenced and seeking to offer new perspectives on heterogeneous catalysts and more sustainable routes for the energy sector, as well as consolidating synthesis by combustion reactions and suggesting a statistical optimization for the process, this work applied the catalysts  $\alpha\text{-MoO}_3$  and  $\alpha/\text{h-MoO}_3$  obtained on a pilot scale through

a combustion reaction in the production of biodiesel from waste cooking oil and ethanol. Using waste oil as a feedstock for biodiesel not only makes the process economically viable, but also avoids competition with edible oils, creating an environmentally friendly solution for disposing of waste cooking oil. The optimized parameters, including reaction time, type of catalyst, and alcohol/oil ratio, were determined using a  $2^3$  experimental design, with 8 experiments and one replication of each, totaling 16 experiments.

## 2. Results

Figure 1a,b illustrates the X-ray patterns of  $\alpha/h$ - $\text{MoO}_3$  and  $\alpha$ - $\text{MoO}_3$  catalysts.

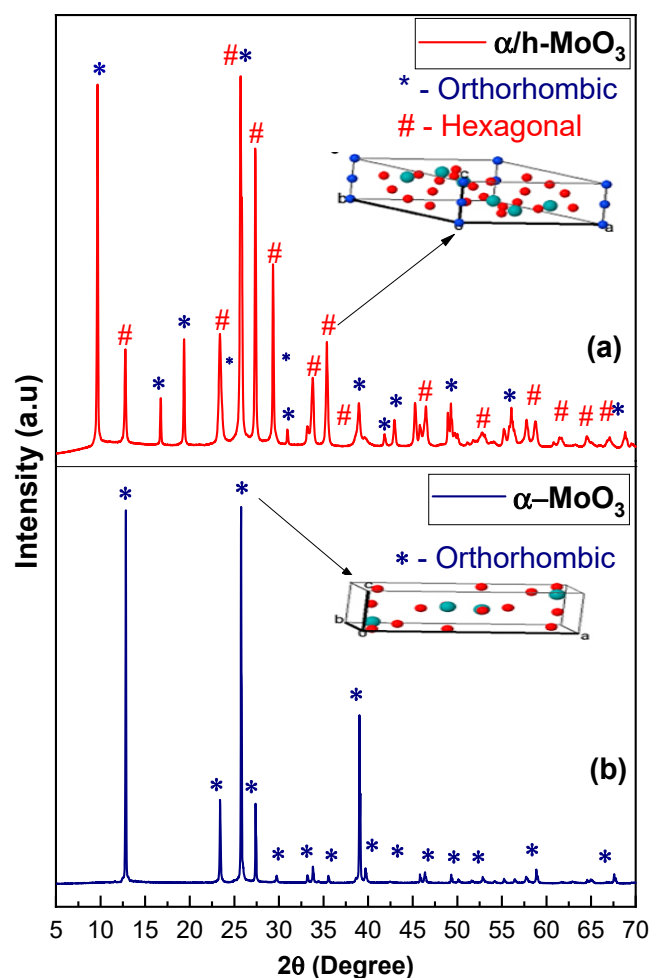


**Figure 1.** X-ray diffraction patterns for  $\text{MoO}_3$  catalysts:  $\alpha/h$ - $\text{MoO}_3$  (a) and  $\alpha$ - $\text{MoO}_3$  (b). Oxygen red; Molybdenum blue.

According to Figure 1, it is evident that the  $\alpha$ - $\text{MoO}_3$  catalyst exhibits a single-phase orthorhombic structure of  $\text{MoO}_3$ , as indicated by the standard chart (PDF2(2019) 00-005-0508), and demonstrates a crystallite size of 84 nm with a crystallinity of 90%. These values surpass those observed for the  $\alpha/h$ - $\text{MoO}_3$  sample, which displays a biphasic structure comprising the hexagonal phase based on the standard reference (PDF2(2019) 00-065-0141), with the second phase corresponding to the orthorhombic crystalline structure of  $\text{MoO}_3$ . The  $\alpha/h$ - $\text{MoO}_3$  sample exhibits a crystallite size and crystallinity of 33 nm and 88%, respectively. These findings suggest that the synthesis via combustion reaction to obtain both single-phase and two-phase  $\text{MoO}_3$  systems was efficient and achievable through a simple and cost-effective method, in contrast to similar studies in the literature utilizing the hydrothermal method for  $\text{MoO}_3$  synthesis. Additionally, successive calcinations post-synthesis were not necessary to achieve an orthorhombic single-phase product [34].

As for the actual density, for the  $\alpha$ -MoO<sub>3</sub> catalyst evidenced by the He pycnometry test, it was 4.5 g/cm<sup>3</sup>, showing little deviation in relation to the theoretical density revealed by the standard crystal chart PDF2(2019) 00-005-0508, which is 4.7 g/cm<sup>3</sup>, thus illustrating the excellent proximity of the material produced in this work to theoretical values. In contrast, the  $\alpha$ /h-MoO<sub>3</sub> catalyst sample presented a natural density of 3.8 g/cm<sup>3</sup>, a different value from that given in the PDF2(2019) 00-065-0141 standard letter of 7.9 g/cm<sup>3</sup>, a fact justified by the mixture of structures that make up the catalyst. Such behavior can be justified by the crystalline arrangement and intercalation of ions in the structure given to MoO<sub>3</sub> materials, where a mixture of orthorhombic and hexagonal phases can cause a difference in the value of the sample's absolute density. Concepts such as density are essential, as density measurements define the mass of catalytic solids that will be used in an industrial reactor [35].

Figure 2 illustrates the thermal events observed from the TGA/DTA curves for the  $\alpha$ /h-MoO<sub>3</sub> and  $\alpha$ -MoO<sub>3</sub> catalysts. Based on this analysis, the temperatures (°C) of decomposition, phase transformation, and mass losses were determined.

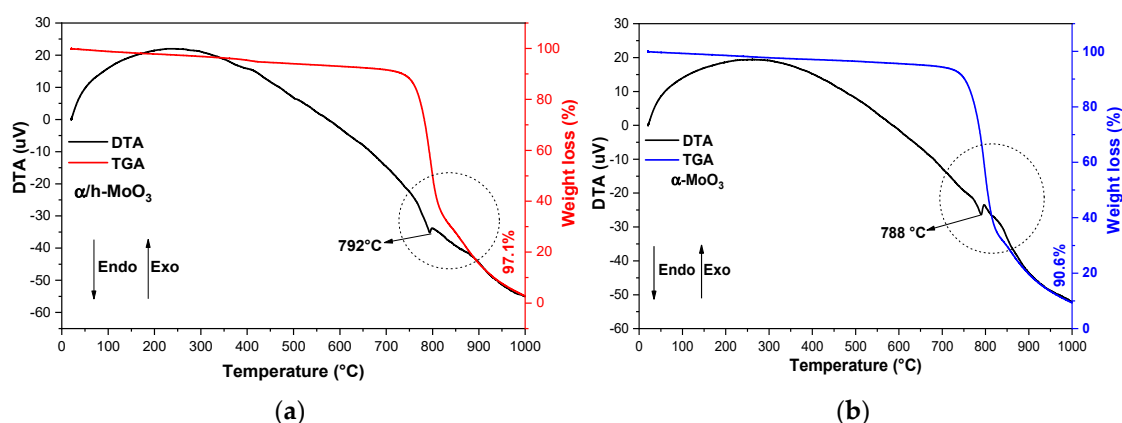


**Figure 2.** TGA/DTA curves for the catalysts:  $\alpha$ /h-MoO<sub>3</sub> (a) and  $\alpha$ -MoO<sub>3</sub> (b).

The catalysts (Figure 2a,b) presented a similar profile to the curves for the TGA/DTA analyses, with thermal events of mass loss and an endothermic peak referring to phase transformation. This also illustrates the thermal stability of the catalysts obtained by combustion reaction at the imposed temperatures. Based on Figure 2a, thermal analysis (TGA) revealed thermal stability verified at temperatures up to ~697 °C, with three consecutive events of mass loss indicating the degradation process for the two-phase catalyst  $\alpha$ /h-MoO<sub>3</sub>, in the temperature range between 372 and 896 °C, with a total mass loss of 97.1%. The DTA curve showed a discrete endothermic peak at temperatures around ~792 °C, which is possibly related to the melting point of the crystalline phase of the orthorhombic phase ( $\alpha$ -MoO<sub>3</sub>), a phase present in the catalyst according to ray diffraction analysis.

As shown in Figure 2b, thermal analysis (TGA) reveals that the thermal stability of the  $\alpha$ -MoO<sub>3</sub> catalyst is observed up to a temperature of ~725 °C; from then on, the degradation process begins through two events of sequential mass loss in the temperature range between 725 and 881 °C, with a total mass loss of 90.6%. The DTA curve illustrates a discrete endothermic peak around 788 °C, which is related to the melting point of the orthorhombic crystalline phase ( $\alpha$ -MoO<sub>3</sub>). The results discussed in this work are very close and compatible with the literature [34,36,37] when studying thermal stability and catalytic characteristics of the  $\alpha$ -MoO<sub>3</sub> crystalline phase.

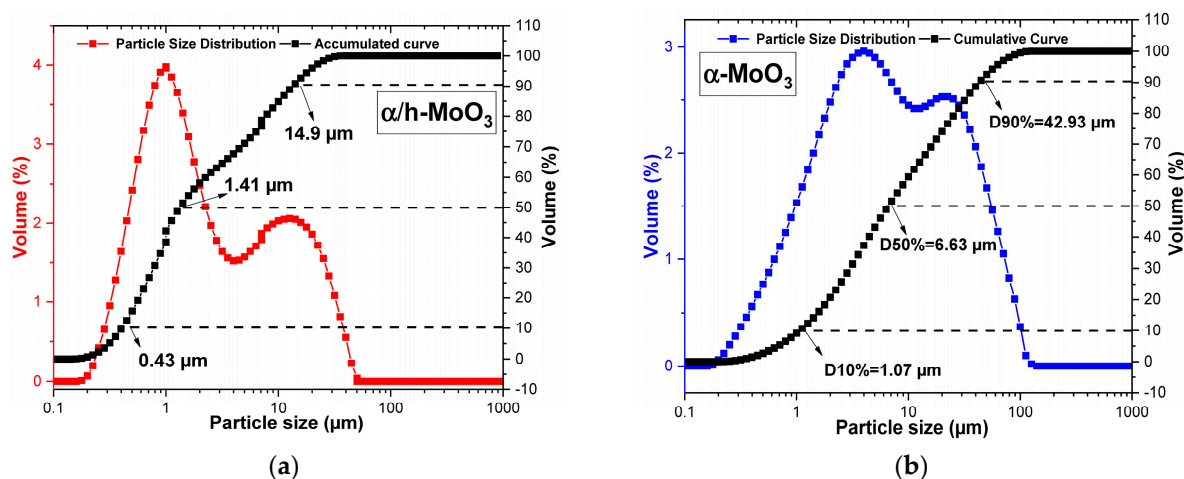
Table 1 describes the experimental values of the semiquantitative analysis of the oxides in the  $\alpha$ /h-MoO<sub>3</sub> and  $\alpha$ -MoO<sub>3</sub> catalysts, determined by EDX.

**Table 1.** Percentages of oxides present by X-ray fluorescence (EDX) for the  $\alpha/h$ -MoO<sub>3</sub> and  $\alpha$ -MoO<sub>3</sub> catalysts.

Oxides Present	Catalysts	
MoO <sub>3</sub>	$\alpha/h$ -MoO <sub>3</sub> 99.79%	$\alpha$ -MoO <sub>3</sub> 99.57%
Fe <sub>2</sub> O <sub>3</sub>	0.21%	0.43%

Based on Table 1, the percentages of oxides present given by X-ray fluorescence (EDX) for the  $\alpha/h$ -MoO<sub>3</sub> and  $\alpha$ -MoO<sub>3</sub> catalysts were (MoO<sub>3</sub>) 99.6% and (Fe<sub>2</sub>O<sub>3</sub>) 0.4%, similar values for the two catalysts under study. The EDX results confirm that molybdenum oxide is the majority element present in the catalysts obtained by combustion reaction, which corresponded to around ~99.6% of the total, followed by traces of iron oxide, which represented around 0.4%, possibly resulting from the preparation process by combustion reaction. The chemical analysis values expressed in this work agree with the studies of [38], when they studied MoO<sub>3</sub> photocatalysts obtained by a method based on Pechini and applied in effluent treatment.

Figure 3 graphically illustrates the particle size analyses, which express the distribution values of the hydrodynamic diameters of the equivalent particles as a function of the cumulative volume for the  $\alpha/h$ -MoO<sub>3</sub> and  $\alpha$ -MoO<sub>3</sub> catalysts.

**Figure 3.** Particle size distribution for the catalysts:  $\alpha/h$ -MoO<sub>3</sub> (a) and  $\alpha$ -MoO<sub>3</sub> (b).

Analyzing Figure 3a,b, it can be seen that the  $\alpha/h$ -MoO<sub>3</sub> and  $\alpha$ -MoO<sub>3</sub> catalysts present a polymodal particle size distribution curve with a wide distribution range for sizes. In the  $\alpha$ -MoO<sub>3</sub> catalyst, it is possible to observe a concentration of particles between ~0.2 and 100  $\mu$ m, with an average particle diameter of 15.43  $\mu$ m being obtained. The accumulated values (black curve in the graph) illustrate an accumulation of particle sizes of 1.07  $\mu$ m up to 10%, 6.63  $\mu$ m up to 50%, and 42.92  $\mu$ m up to 90%.

For the  $\alpha/h$ -MoO<sub>3</sub> catalyst, a concentration of hydrodynamic particle sizes slightly below 100  $\mu$ m was observed, and a difference was observed between the synthesized samples. Another aspect that differs from the single-phase sample is the average particle size values of 7.7  $\mu$ m and accumulated values of 0.43, 1.41, and 14.9  $\mu$ m for the accumulated values D10, D50, and D90, respectively. The values observed for the  $\alpha$ -MoO<sub>3</sub> sample are lower or lower when compared to the two-phase catalyst. According to XRD analysis, this phenomenon can possibly be justified by the presence of two distinct morphologies of MoO<sub>3</sub>.

Figure 4 illustrates the Raman spectra of MoO<sub>3</sub> catalysts synthesized in this work.



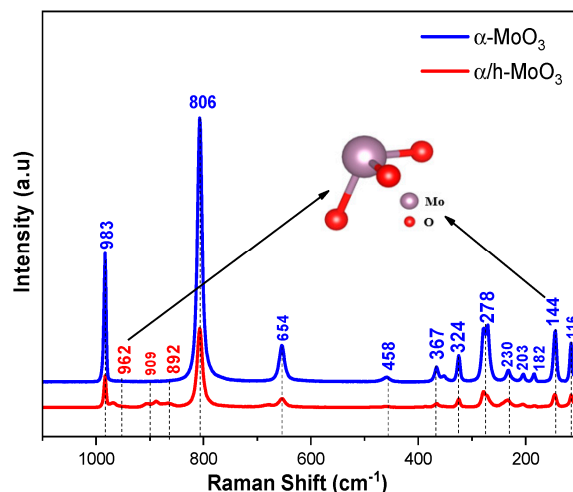


**Figure 4.** Raman spectroscopy of  $\alpha$ -MoO<sub>3</sub> and  $\alpha$ /h-MoO<sub>3</sub> catalysts.

The attributions observed in the Raman spectra (Figure 4) were based on those described in the literature [39–42]. The vibrational modes appearing around 600–1000 cm<sup>−1</sup> correspond to the stretching vibrations of the MoO<sub>6</sub> octahedron, while modes between 200 and 400 cm<sup>−1</sup> originate from the bending vibrations of the MoO<sub>6</sub> octahedron. Modes below 200 cm<sup>−1</sup> are attributed to the deformation of the network of MoO<sub>6</sub> octahedra, referring to the orthorhombic crystal configuration of MoO<sub>3</sub> [39,42]. The bands observed in the range of 968–884 cm<sup>−1</sup>, seen as a distinguishing feature in the  $\alpha$ /h-MoO<sub>3</sub> sample, likely correspond to the elastic vibrations of the MoO<sub>6</sub> octahedron in the hexagonal crystal structure of MoO<sub>3</sub>, corroborating the studies by Lopez et al. [42]. Such behavior was also noted by Zhang et al. [41], confirming the XRD results (Figure 1), which indicated that the catalyst is formed by two crystalline phases of MoO<sub>3</sub>.

The particle size values observed in this work differ from the recent literature consulted, which reports a nanometer scale for the particle size obtained by synthetic methods similar to that presented in this work [43–45].

Figure 5a,b illustrates the images obtained by scanning electron microscopy (SEM) of the  $\alpha$ /h-MoO<sub>3</sub> and  $\alpha$ -MoO<sub>3</sub> catalysts obtained by the combustion reaction method.

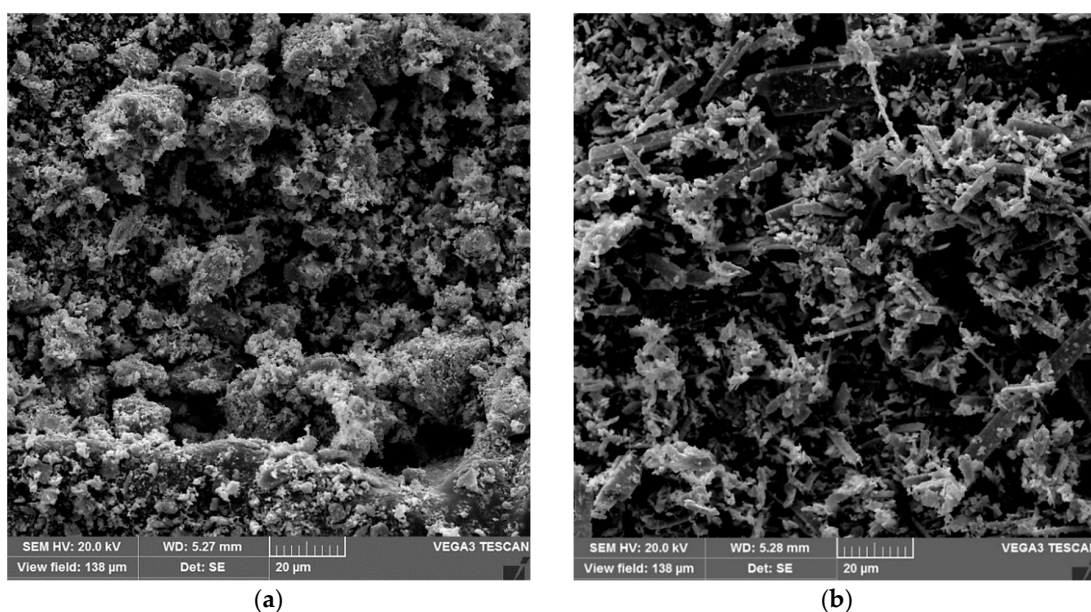


**Figure 5.** Morphologies obtained by SEM at 1500 $\times$  for the support material  $\alpha$ /h-MoO<sub>3</sub> (a) and  $\alpha$ -MoO<sub>3</sub> (b).

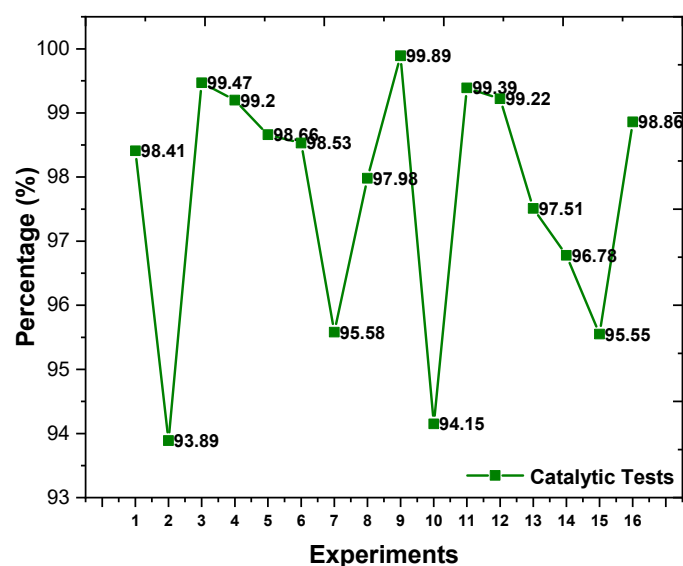
It is possible to observe that the  $\alpha$ /h-MoO<sub>3</sub> two-phase catalyst (Figure 5a) illustrates a mixed morphology with highly agglomerated short plates with apparent porosity possibly arising from the combustion synthesis process; the  $\alpha$ -MoO<sub>3</sub> single-phase catalyst (Figure 5b), illustrates elongated prismatic morphologies, with flat faces and well-defined edges, both with a wide range of cluster sizes, according to the granulometric distribution discussed and the recent literature studies [34].

Table 2 describes and Figure 6 illustrates the experimental design response 2<sup>3</sup> used to analyze and optimize the statistical data of biodiesel production.

**Table 2.** 2<sup>3</sup> factorial experimental design response obtained for the random variables time, type of catalyst, alcohol/oil ratio, and conversion to ester.

Experiment	(1) Time (min)	(2) Type of Catalyst	(3) Alcohol/Oil Ratio	Y = Conversion to Ester (%)
1	60	$\alpha$ /h-MoO <sub>3</sub>	1/15-	98.41
2	120	$\alpha$ /h-MoO <sub>3</sub>	1/15	93.89
3	60	$\alpha$ -MoO <sub>3</sub>	1/15	99.47
4	120	$\alpha$ -MoO <sub>3</sub>	1/15	99.20
5	60	$\alpha$ /h-MoO <sub>3</sub>	1/20	98.66
6	120	$\alpha$ /h-MoO <sub>3</sub>	1/20	98.53
7	60	$\alpha$ -MoO <sub>3</sub>	1/20	95.58
8	120	$\alpha$ -MoO <sub>3</sub>	1/20	97.98
9(R) *	60	$\alpha$ /h-MoO <sub>3</sub>	1/15	99.89
10(R) *	120	$\alpha$ /h-MoO <sub>3</sub>	1/15	94.15
11(R) *	60	$\alpha$ -MoO <sub>3</sub>	1/15	99.39
12(R) *	120	$\alpha$ -MoO <sub>3</sub>	1/15	99.22
13(R) *	60	$\alpha$ /h-MoO <sub>3</sub>	1/20	97.51
14(R) *	120	$\alpha$ /h-MoO <sub>3</sub>	1/20	96.78
15(R) *	60	$\alpha$ -MoO <sub>3</sub>	1/20	95.55
16(R) *	120	$\alpha$ -MoO <sub>3</sub>	1/20	98.86

\* (R) Replicate. Highlighted the best conversions in planning ester.



**Figure 6.** Percentage results of converting residual oil into ethyl esters obtained in the presence of  $\alpha$ -MoO<sub>3</sub> and h/ $\alpha$ -MoO<sub>3</sub> catalysts.

It can be seen in Table 2 and Figure 6 that the  $\alpha$ -MoO<sub>3</sub> catalyst and an oil/alcohol ratio of 1/15 at an occurrence time of 60 min (Experiment 3) tend to provide higher conversion

rates to ester. However, the catalysts synthesized by combustion reaction were active under all conditions tested and the conversions into fatty acid esters varied between 93 and 99%.

The statistical study was carried out based on the observed reaction data (Table 2). The Pareto chart (Figure 7) was initially used as a response to the statistical analysis of experimental design  $2^3$  to optimize the TES conditions of the residual oil catalyzed by  $\alpha/h\text{-MoO}_3$  and  $\alpha\text{-MoO}_3$ .

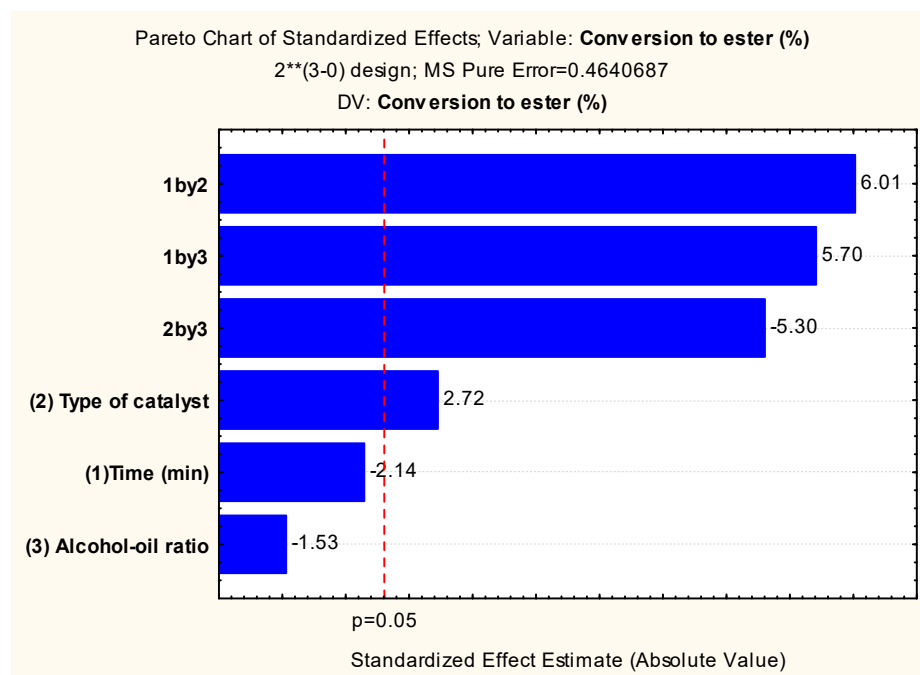


**Figure 7.** Pareto chart resulting from the  $2^3$  factorial planning for converting waste oil into biodiesel. \*\* High.

It is possible to observe in Figure 6 that among the input variables, the most significant first order was the type of catalyst followed by all interactions of all other variables (oil/alcohol ratio and reaction time), with 95% reliability ( $p < 0.05$ ) and with positive interference (+1) from the catalyst type variable, that is, the  $\alpha\text{-MoO}_3$  catalyst presents a statistically significant interference to the process. The variables time and alcohol/oil ratio did not show a statistically significant effect. These observations corroborate the data in Table 2 and Figure 7, suggesting that the use of the single-phase catalyst significantly increases the conversion of residual oil into biodiesel.

Level curves of the experimental planning response were also obtained, using as independent variables the type of catalyst and alcohol/oil ratio, and are illustrated in Figure 8.

The type of catalyst in the conversion reaction of residual oil into ethyl esters was better evaluated when using longer reaction times (+1) (120 min) and use of the single-phase catalyst (+1); at this point, the biodiesel conversion was at the maximum (close to 100%), corroborating what was observed in the Pareto chart (Figure 7).

In the region investigated, the response surface is satisfactorily described by the linear mathematical model given by Equation (1), which presented an  $R^2$  of 92% and which defines the plane represented in perspective on the level curve (Figure 8), based on the experimental planning carried out and which best describes the data collected and adjusted to the data in Table 2.

$$Z_{(x,y)} = 97.691875 - 0.365625 \times x + 0.464375 \times y + 1.024375 \times x \times y + 0.971875 \times 0.*x - 0.903125 \times 0.*y + 0 \quad (1)$$



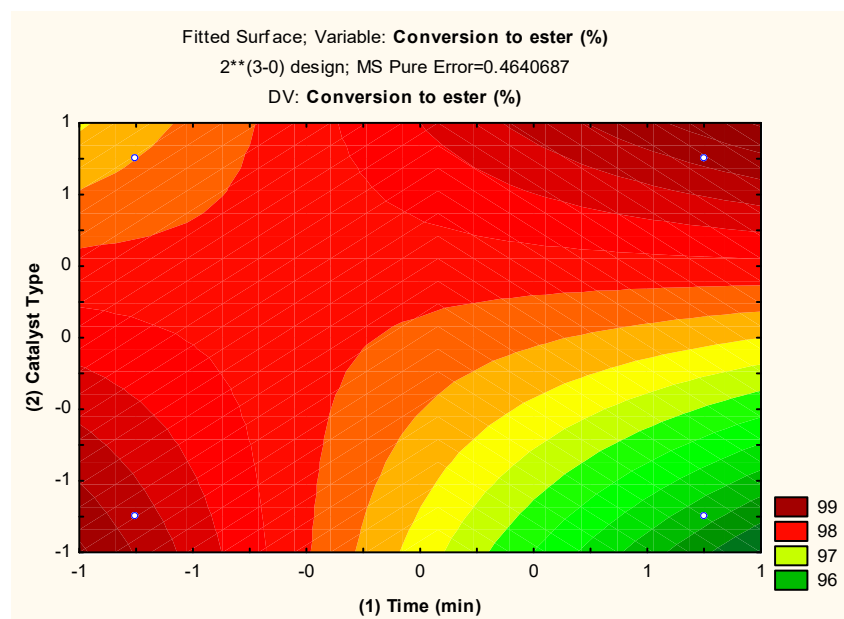


**Figure 8.** Conversion level curve of residual oil into biodiesel with the interaction between (2) type of catalyst and (1) time (min). \*\* High.

The data illustrated in Figures 7 and 8 and the linear equation (Equation (1)) indicate that the statistical model adopted represents a good description of the experimental data related to the ethyl ester content in the reaction time of 1 h, oil/alcohol ratio 1/15, 4% catalyst, and temperature of 200 °C. These conditions were revealed as optimal by the statistical model used. The fit of the quadratic model was also tested by analysis of variance (ANOVA) according to Table 3.

**Table 3.** ANOVA to optimize biodiesel production from waste oil using an  $\alpha$ -MoO<sub>3</sub> catalyst.

ANOVA Table				
Source of Variation	Quadratic Sum	Degrees of Freedom	Quadratic Mean	
Regression	51.63	6	8.60	$F_{\text{cal. of regression}} 17.71$
Waste	4.37	9	0.49	$F_{\text{calc. of (Lack of fit)}} 1.42$
Lack of adjustment	0.66	1	0.66	
Pure error	3.71	8	0.46	
Total	56.00	15		
$F_{\text{tabelado REG}}$	3.37	$F_{\text{cal}}/F_{\text{tab}}$ (Regression)	5.25	
$F_{\text{tabelado da F. Aj}}$	5.32	$F_{\text{cal}}/F_{\text{tab}}$ (Lack of fit)	0.27	
%Mx. explained	92.19	Model Statistics		
%Mx. explainable	93.37	$R^2$ (%)	92.19	
$R^2$	0.92	$R^2$ adjusted (%)	76.44	
Fit quality	0.76	$F_{\text{calc}}/F_{\text{tab}}$ (regression)	5.25	
S (standard error of regression)	0.70	$F_{\text{calc}}/F_{\text{tab}}$ (lack of fit)	0.27	
		Regression standard error	0.70	

The results expressed in the ANOVA (Table 3) presented a value for  $F_{\text{cal}}/F_{\text{tab}}$  of 5.25 for the regression, indicating that the model was statistically significant, and the value for  $F_{\text{cal}}/F_{\text{tab}}$  of lack of adjustment of 0.27, indicating that the model was predictive, so the F test revealed that the planning used was predictive and significant. Therefore, the regression model given by Equation (1) was a reasonable predictor of the experimental results, and the influenced factors were real with a confidence level of 95%, as already observed in Figure 6.

The optimal condition revealed by experimental planning <sup>23</sup>, which is in line with Figures 6–8, Equation (1), and Tables 2 and 3, is level -1 for the time variable (60 min), 1 for the type of catalyst ( $\alpha$ -MoO<sub>3</sub>), and level -1 for the alcohol/oil molar ratio (1:15), indicating

biodiesel conversions of ~99% with an overall desirability (~1) of 0.95, which illustrates that the optimization method used was efficient. Similar statistical behaviors were observed in the works of G. Novaes, T. Yamaki, F. de Paula, B. do Nascimento Júnior, A. Barreto, S. Valasques, and A. Bezerra [31], and Paula and Fernandes [46] when they used statistical planning to optimize variables that influence the performance of analytical methods and optimize water treatment, respectively.

The optimal conversion condition for esters, the  $\alpha$ -MoO<sub>3</sub> catalyst, was recovered and reused in the TES reaction (conditions: 30% residual oil mass, 1-hour time, alcohol/oil ratio 15:1, 4% catalyst mass, and 200 °C). The conversion results obtained with the reuse are illustrated in Figure 9.

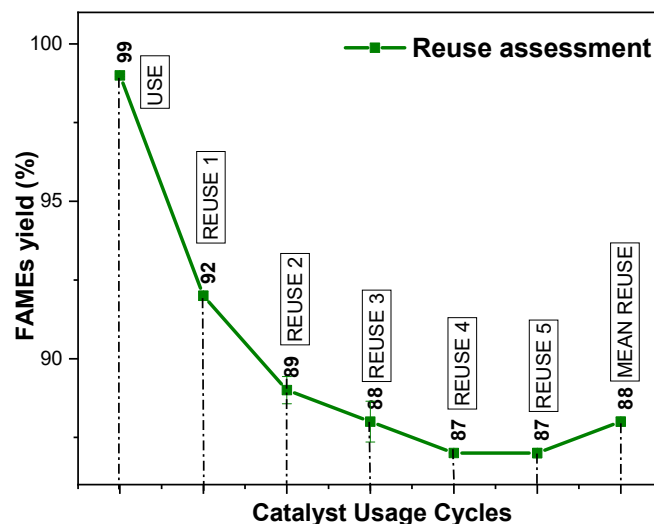


Figure 9. Results of reuse tests obtained for the  $\alpha$ -MoO<sub>3</sub> catalyst' in TES reactions.

Based on Figure 9, the catalyst initially exhibited very high efficiency with a conversion to ethyl esters of 99% and a relatively low deviation of 0.04. This indicates that the catalyst was actively functioning in the first reaction it was used in.

As the catalyst was reused, a gradual decrease in its effectiveness was observed. Conversion decreased from 92 in the first reuse to 87 in the fourth and fifth reuses. Additionally, the deviations increased significantly over the reuses, indicating greater variability in the results as well as a change in its coloration over the reuse cycles.

Despite the decrease in effectiveness over the reuses, the average of the results still remains relatively high, around 88. However, the standard deviation remains at 0.14, suggesting that there is still a significant amount of variation in the results.

These data indicate that although the catalyst maintains a reasonably average effectiveness over the reuses, there is a slight trend towards decreased performance. This could be attributed to various factors such as accumulation of impurities, structural changes in the catalyst, or poisoning of the catalyst by undesired reaction products.

### 3. Materials and Methodology

#### 3.1. Materials

The following materials were used in the synthesis of catalysts based on MoO<sub>3</sub>: Ammonium heptamolybdate—(NH<sub>4</sub>)<sub>6</sub>Mo<sub>7</sub>O<sub>24</sub>·4 H<sub>2</sub>O (99% purity, Sigma-Aldrich—Saint Louis, MO, USA), urea—CO(NH<sub>2</sub>)<sub>2</sub> (99% purity, Dynamic—São Paulo, Brazil), nitric acid—HNO<sub>3</sub> (65% purity, Nuclear—Rio de Janeiro, Brazil), ethylic alcohol—CH<sub>3</sub>CH<sub>2</sub>OH (99.5% purity, Dynamic), and *n*-hexane—C<sub>6</sub>H<sub>14</sub> (99%, Neon São Paulo, Brazil). They were used as received without further purification. The residual oil used was collected in pastry shops in Campina Grande, located in Paraíba state, Brazil. Before experiments, the as-received residual oil was filtered (filter paper C15.00 ± 0.15 cm) to remove the suspended particulate matter. The oil showed fatty acid composition typical of soybean oil (12% of palmitic acid

(16:0), 4% of stearic acid (18:0), 1% of oleic acid (18:1), 54% of linoleic acid (18:2), and 12% of linolenic acid (18:3)). The residual oil acidity was 6.79 0.05 mgKOH/g sample.

### 3.2. Methods

#### 3.2.1. Synthesis of Catalysts

The stoichiometry of the precursor reaction solution for MoO<sub>3</sub> was calculated based on the total valence of oxidizing and reducing agents [47]. Ammonium heptamolybdate (AHM) ((NH<sub>4</sub>)<sub>6</sub>Mo<sub>7</sub>O<sub>24</sub> 4H<sub>2</sub>O) was used as the metallic precursor, with the valences of the reactive elements as follows: C = +4; H = +1; N = 0; O = −2; and Mo = +6. Mo and O were considered oxidizing elements, while urea (CO(NH<sub>2</sub>)<sub>2</sub>) was considered the reducing agent (fuel). For maximum energy release, all oxygen content in the metallic precursor must oxidize, leading to a zero oxygen balance. Assuming a 1:1 stoichiometry, the synthesis requires an equivalent amount of “n” moles of fuel, where n = 0.03/6 = 0.005 moles of urea. Thus, the balanced theoretical chemical reaction for the synthesis of the MoO<sub>3</sub> system can be expressed by Equation (2).



The catalysts were synthesized via combustion reaction in a stainless steel container, coded P08, and prepared to obtain powders with a batch production of 20 g, following the device and methodology patent INPI: BR10 2021 018179-6 [48] and the combustion reaction synthesis architecture described in the patent device INPI: BR 10 2012 002181-3 [49].

#### 3.2.2. Catalytic Test

The performance of MoO<sub>3</sub> catalysts was evaluated in the synthesis of biodiesel using waste oil via TES reaction. The catalytic tests were conducted in a stainless-steel pressurized system reactor (Parr 4848) with a capacity of 100 mL, mechanical stirrer, time and temperature controller, and pressure indicator. After the TES reactions, the catalysts were separated from the products in a centrifuge (3500 rpm) and subsequently purified with n-hexane, washed with distilled water at ~70 °C, and then dried in an oven at 110 °C/24 h. The biodiesel produced was washed with distilled water at ~70 °C and dried in an oven at 110 °C for 30 min with manual stirring at 5 min intervals.

#### 3.2.3. Catalyst Reuse

After the reaction, the catalysts were collected, washed with n-hexane, and dried in an oven at 110 °C for 24 h and then reserved for sequential reuse. The reuse tests were accomplished under the best reactive conditions established from the results of the catalytic tests.

#### 3.2.4. Statistical Analysis

For the analysis and optimization of the biodiesel synthesis process from waste oil, a 2<sup>3</sup> factorial experimental design was prepared with 8 experiments with one replication (duplicate injection for gas chromatography analysis), totaling 16 random experiments, which were analyzed using a Pareto chart, level curves, and ANOVA table, and were evaluated in the *Statistic 7.0* program. Table 4 describes the input levels and variables for the proposed experimental design.

**Table 4.** Variables and input levels proposed for experimental planning 2<sup>3</sup>.

Variables	Levels	
	−1	+1
(1) Time (min)	60	120
(2) Type of catalyst	α/h-MoO <sub>3</sub>	α-MoO <sub>3</sub>
(3) Alcohol/oil ratio	15:1	20:1

**Fixed conditions:** Temperature 200 °C, 30 g of residual oil, and 4% catalyst.

Time, type of catalyst, and oil/alcohol ratio are considered in the factorial experimental design  $2^3$ . The two levels for the selected factors were determined from preliminary exploratory experiments and assistance from the recent published literature [34,50,51]. The planning matrix (Table 5) was obtained from the choice of variables and levels with the help of the *Statistic 7.0* software, which was used to analyze the experiments using level curves, the ANOVA table, and the Pareto.

**Table 5.**  $2^3$  factorial planning matrix with replication for the catalytic test experiments.

Experiment	(1) Time (min)	(2) Type of Catalyst	(3) Alcohol/Oil Ratio
1	−	−	−
2	+	−	−
3	−	+	−
4	+	+	−
5	−	−	+
6	+	−	+
7	−	+	+
8	+	+	+
9(R) *	−	−	−
10(R) *	+	−	−
11(R) *	−	+	−
12(R) *	+	+	−
13(R) *	−	−	+
14(R) *	+	−	+
15(R) *	−	+	+
16(R) *	+	+	+

\* (R) Replica of injection in the chromatograph.

The conversion of residual oil into biodiesel (Y) was used as a response to determine the optimized parameters. The effect of independent factors on dependent factors was analyzed using a linear equation (Equation (3)), following the suggestion of a linear configuration for the proposed planning:

$$Y = \alpha_0 + \sum_{i=1}^k \alpha_i X_i + \sum_{i < j}^k \alpha_{ij} X_i X_j + e \quad (3)$$

where Y is the ester content response variable;  $\alpha_0$  is the compensated term;  $\alpha_i$  is the first order linear coefficient;  $\alpha_{ij}$  is the linear interaction coefficient between variables, and refers to the pure error associated with the experiments; and  $X_i$  and  $X_j$  are input variables.

### 3.2.5. Characterizations

The  $\alpha$ - $\text{MoO}_3$  catalyst was characterized by X-ray diffraction (XRD) using a BRUKER (Billerica, MA, USA) X-ray diffractometer (model D2 PHASER, Cu-K $\alpha$  radiation), operating with 30 kV and 10 mA, with copper K $\alpha$  radiation source ( $k\alpha = 1.54056 \text{ \AA}$ ). The sweep range used at  $2\theta = 10^\circ$  at  $70^\circ$ , with an angular step of  $0.016^\circ$  and a counting time of 1.000 s per step. The crystalline phases identification were carried out from the ICDD crystallographic records of the PDF2/2019 database with the aid of *DiffraPlus Suite Eva* software V 7, which was also used to obtain the crystallinity values and the size of the crystallite (calculated with the aid of the Scherrer equation) [52].

Raman spectra were recorded on a RENISHAW (West Dundee, IL, USA) spectrophotometer (model InVia Raman microscope) using an Ar<sup>+</sup> laser, with a power of 100 mW and a wavelength of 514 nm. The 50 $\times$  objective was used. Raman spectra were obtained under room temperature, in the frequency ranges of 90–1200  $\text{cm}^{-1}$ .

The actual density value of the catalyst was obtained through the analysis with a Quantachrome Corporation (Boynton Beach, FL, USA) Upyc 1200e v5.04 Pycnometer operating with helium gas (He). Thermogravimetric analysis (TGA/DTA) was evaluated using a Shimadzu (Tokyo, Japan) TA 60H simultaneous thermal analysis system, with a heating rate of 12.5  $^\circ\text{C}/\text{min}$  under air atmosphere 100 mL/min (maximum temperature 1000  $^\circ\text{C}$ ).

The semi-quantitative analysis of the oxides and elements present in the samples were determined by energy dispersive X-ray fluorescence spectroscopy, model EDX-720, from Shimadzu. The laser diffraction particle size analysis uses the liquid phase particle dispersion method associated with an optical measurement process through laser diffraction on the Mastersizer 2000 equipment from Malvern (Worcestershire, UK). The morphological aspects of the catalyst sample were acquired by scanning electron microscopy (SEM), brand Tescan (Brno, Czech Republic), model Vega3.

The percentages of ethyl esters were determined by gas chromatography using a VARIAN (Las Vegas, NV, USA) 450c instrument chromatograph with flame ionization detector and capillary column as stationary phase (Varian Ultimetel "Select Biodiesel Glycerides RG"; dimensions: 15 m × 0.32 mm × 0.45 mm). The initial injection and oven temperatures were 100 °C and 180 °C, respectively, and the detector operated at 380 °C.

#### 4. Conclusions

Combustion synthesis has proven to be highly effective in producing catalysts. MoO<sub>3</sub>-based catalysts were obtained in orthorhombic and hexagonal phases, with crystal sizes ranging from 35 to 81 nm and crystallinity between 88% and 90%. Additionally, they exhibited remarkable thermal stability, enduring temperatures up to 800 °C. Molybdenum oxide emerged as the predominant component in these catalysts.

During catalytic activity tests, the catalysts showed efficiency under all evaluated reaction conditions. Remarkably, the monophasic  $\alpha$ -MoO<sub>3</sub> catalyst displayed slight superiority in catalytic activity, achieving a 99% conversion for ethyl esters at 200 °C for one hour, with a catalyst concentration of 4% by mass of ethanol/oil, and a molar ratio of 15:1.

Furthermore, this monophasic catalyst proved to be recyclable, maintaining a lifespan of up to six cycles with an average reuse of 88%. The use of factorial design allowed for a more in-depth analysis of the involved variables (catalyst type, alcohol/oil ratio, and time), revealing that catalyst type had the most significant influence on the residual oil's TES. The adopted statistical model was both significant and predictive, with a significance level of 95%.

The optimal conditions determined by experimental design resulted in high conversions to biodiesel, demonstrating the efficacy of the linear optimization employed. These findings align with the existing literature and underscore the viability of using  $\alpha$ -MoO<sub>3</sub> catalysts in biodiesel production from residual oil, employing optimization strategies to achieve the best catalytic outcomes possible. The catalysts developed in this study exhibit a high potential for industrial applications, especially when compared to residual oil and the ethanol routes, thus potentially making positive contributions to the environment and global society at large.

**Author Contributions:** Conceptualization, A.L.d.S. and C.B.B.L.; methodology, D.G.G. and H.d.L.P.; software; J.K.D.; validation, H.B.S. and A.L.d.S.; formal analysis, A.L.d.S. and H.d.L.P.; investigation, A.L.d.S. and H.d.L.P.; resources, A.C.F.d.M.C.; data curation, C.B.B.L.; writing—preparation of the original draft, M.C.F.A. and H.d.L.P.; writing—review and editing, M.C.F.A.; visualization, A.C.F.d.M.C.; supervision, M.C.F.A.; project administration, A.C.F.d.M.C.; acquisition of financing, A.C.F.d.M.C. All authors have read and agreed to the published version of the manuscript.

**Funding:** The authors acknowledge the financing of this research by CNPq (National Council for Scientific and Technological Development). Process 150292/2022-8 (Adriano Lima da Silva) and process 350025/2023-1 (Carlos Bruno Barreto Luna). We thank Carlos Bruno Barreto Luna for his contributions to improving the manuscript, as well as the feasibility of publishing the manuscript.

**Informed Consent Statement:** Not applicable.

**Data Availability Statement:** Data are contained within the article.

**Acknowledgments:** The authors wish to thank CAPES (Coordination for the Improvement of Higher Education Personnel) and CNPq (National Council for Scientific and Technological Development) for the scholarships.



**Conflicts of Interest:** The authors declare no conflict of interest.

## References

1. Abbasi, T.U.; Ahmad, M.; Asma, M.; Rozina; Munir, M.; Zafar, M.; Katubi, K.M.; Alsaiani, N.S.; Yahya, A.E.M.; Mubashir, M.; et al. High efficient conversion of *Cannabis sativa* L. biomass into bioenergy by using green tungsten oxide nano-catalyst towards carbon neutrality. *Fuel* **2023**, *336*, 126796. [[CrossRef](#)]
2. Malpartida, I.; Maireles-Torres, P.; Vereda, C.; Rodriguez-Maroto, J.M.; Halloumi, S.; Lair, V.; Thiel, J.; Lacoste, F. Semi-continuous mechanochemical process for biodiesel production under heterogeneous catalysis using calcium diglycerate. *Renew. Energy* **2020**, *159*, 117. [[CrossRef](#)]
3. Farokhi, G.; Saidi, M. Catalytic activity of bimetallic spinel magnetic catalysts ( $\text{NiZnFe}_2\text{O}_4$ ,  $\text{CoZnFe}_2\text{O}_4$  and  $\text{CuZnFe}_2\text{O}_4$ ) in biodiesel production process from neem oil: Process evaluation and optimization. *Chem. Eng. Process. Process Intensif.* **2022**, *181*, 109170. [[CrossRef](#)]
4. Karmakar, B.; Ghosh, B.; Samanta, S.; Halder, G. Sulfonated catalytic esterification of *Madhuca indica* oil using waste *Delonix regia*: L16 Taguchi optimization and kinetics. *Sustain. Energy Technol. Assess.* **2020**, *37*, 100568. [[CrossRef](#)]
5. Ganesha, T.; Prakash, S.B.; Rani, S.S.; Ajith, B.S.; Patel, G.C.M.; Samuel, O.D. Biodiesel yield optimization from ternary (animal fat-cotton seed and rice bran) oils using response surface methodology and grey wolf optimizer. *Ind. Crops Prod.* **2023**, *206*, 117569. [[CrossRef](#)]
6. Karimi, S.; Saidi, M. Converting neem seed-derived oil into biodiesel using zeolite ZSM-5 as an efficient catalyst via electrosynthesis procedure: Optimization of operating variables using response surface methodology (RSM). *Process Saf. Environ. Prot.* **2024**, *183*, 111. [[CrossRef](#)]
7. Hasannia, S.; Kazemini, M.; Seif, A. Optimizing parameters for enhanced rapeseed biodiesel production: A study on acidic and basic carbon-based catalysts through experimental and DFT evaluations. *Energy Convers. Manag.* **2024**, *303*, 118201. [[CrossRef](#)]
8. Grosman, M.T.; Andrade, T.A.; Bitonto, L.D.; Pastore, C.; Corazza, M.L.; Tronci, S.; Errico, M. Hydrated metal salt pretreatment and alkali catalyzed reactive distillation: A two-step production of waste cooking oil biodiesel. *Chem. Eng. Process Process Intensif.* **2022**, *176*, 108980. [[CrossRef](#)]
9. Ibrahim, S.M. Preparation, characterization and application of novel surface-modified  $\text{ZrSnO}_4$  as Sn-based TMOs catalysts for the stearic acid esterification with methanol to biodiesel. *Renew. Energy* **2021**, *173*, 151. [[CrossRef](#)]
10. Lin, X.; Li, M.; Chen, Z.; Li, M.; Huang, Y.; Qiu, T. One-step fabrication of polymeric self-solidifying ionic liquids as the efficient catalysts for biodiesel production. *J. Clean. Prod.* **2021**, *292*, 125967. [[CrossRef](#)]
11. Albuquerque, A.A.; Ng, F.T.T.; Danielski, L.; Stragevitch, L. A new process for biodiesel production from tall oil via catalytic distillation. *Chem. Eng. Res. Des.* **2021**, *170*, 314. [[CrossRef](#)]
12. Al-Mawali, K.S.; Osman, A.I.; Al-Muhtaseb, A.A.H.; Mehta, N.; Jamil, F.; Mjalli, F.; Vakili-Nezhaad, G.R.; Rooney, D.W. Life cycle assessment of biodiesel production utilising waste date seed oil and a novel magnetic catalyst: A circular bioeconomy approach. *Renew. Energy* **2021**, *170*, 832. [[CrossRef](#)]
13. Zhang, G.; Xie, W. ZrMo oxides supported catalyst with hierarchical porous structure for cleaner and sustainable production of biodiesel using acidic oils as feedstocks. *J. Clean. Prod.* **2023**, *384*, 135594. [[CrossRef](#)]
14. Elouahed, S.K.; Asikin-Mijan, N.; Alsultan, G.A.; Kaddour, O.; Yusop, M.R.; Mimoun, H.; Samidin, S.; Mansir, N.; Taufiq-Yap, Y.H. Optimization of the activity of  $\text{Mo}_7\text{-Zn}_3/\text{CaO}$  catalyst in the transesterification of waste cooking oil into sustainable biodiesel via response surface methodology. *Energy Convers. Manag.* **2024**, *303*, 118185. [[CrossRef](#)]
15. Amirkhanyan, N.; Kirakosyan, H.; Zakaryan, M.; Zurnachyan, A.; Rodriguez, M.A.; Abovyan, L.; Aydinyan, S. Sintering of silicon carbide obtained by combustion synthesis. *Ceram. Int.* **2023**, *49*, 26129. [[CrossRef](#)]
16. Betinelli, G.A.D.A.; Modolon, H.B.; Wermuth, T.B.; Raupp-Pereira, F.; Montedo, O.R.K.; Vassen, A.B.; Demétrio, K.B.; Arcaro, S. Combustion synthesis of nanostructured calcium silicates: A new approach to develop bioceramic cements in endodontics. *Ceram. Int.* **2024**, *50*, 4544. [[CrossRef](#)]
17. Chudakova, M.V.; Popov, M.V.; Korovchenko, P.A.; Pentsak, E.O.; Latypova, A.R.; Kurmashov, P.B.; Pimenov, A.A.; Tsilimbaeva, E.A.; Levin, I.S.; Bannov, A.G.; et al. Effect of potassium in catalysts obtained by the solution combustion synthesis for co-production of hydrogen and carbon nanofibers by catalytic decomposition of methane. *Chem. Eng. Sci.* **2024**, *284*, 119408. [[CrossRef](#)]
18. Silva, A.L.; Farias, A.F.F.; Pontes, J.R.M.; Rodrigues, A.M.; Costa, A.C.F.D.M. Synthesis of the  $\text{ZnO-Ni}_{0.5}\text{Zn}_{0.5}\text{Fe}_2\text{O}_4\text{-Fe}_2\text{O}_3$  magnetic catalyst in pilot-scale by combustion reaction and its application on the biodiesel production process from oil residual. *Arab. J. Chem.* **2020**, *13*, 7665. [[CrossRef](#)]
19. Alanis, C.; Córdoba, L.I.Á.; Álvarez-Arteaga, G.; Romero, R.; Padilla-Rivera, A.; Natividad, R. Strategies to improve the sustainability of the heterogeneous catalysed biodiesel production from waste cooking oil. *J. Clean. Prod.* **2022**, *380*, 134970. [[CrossRef](#)]
20. Wang, Q.; Wenlei, X.; Guo, L. Molybdenum and zirconium oxides supported on KIT-6 silica: A recyclable composite catalyst for one-pot biodiesel production from simulated low-quality oils. *Renew. Energy* **2022**, *187*, 907. [[CrossRef](#)]
21. Sebayang, A.H.; Kusumo, F.; Milano, J.; Shamsuddin, A.H.; Silitonga, A.S.; Ideris, F.; Siswantoro, J.; Veza, I.; Mofijur, M.; Chia, S.R. Optimization of biodiesel production from rice bran oil by ultrasound and infrared radiation using ANN-GWO. *Fuel* **2023**, *346*, 128404. [[CrossRef](#)]

22. Alotaibi, M.A.; Naeem, A.; Khan, I.W.; Farooq, M.; Din, I.U.; Saharun, M.S. Optimization and cost analysis evaluation studies of the biodiesel production from waste cooking oil using Na–Si/Ce-500 heterogeneous catalyst. *Biomass Bioenergy* **2024**, *182*, 107078. [[CrossRef](#)]
23. Xie, W.; Gao, C.; Li, J. Sustainable biodiesel production from low-quantity oils utilizing H6PV3MoW8O40 supported on magnetic Fe<sub>3</sub>O<sub>4</sub>/ZIF-8 composites. *Renew. Energy* **2021**, *168*, 927. [[CrossRef](#)]
24. Abdelbasset, W.K.; Alrawaili, S.M.; Elsayed, S.H.; Diana, T.; Ghazali, S.; Felemban, B.F.; Zwawi, M.; Algarni, M.; Su, C.-H.; Nguyen, H.C.; et al. Optimization of heterogeneous Catalyst-assisted fatty acid methyl esters biodiesel production from Soybean oil with different Machine learning methods. *Arab. J. Chem.* **2022**, *15*, 103915. [[CrossRef](#)]
25. Badia, J.H.; Ramírez, E.; Soto, R.; Bringué, R.; Tejero, J.; Cunill, F. Optimization and green metrics analysis of the liquid-phase synthesis of sec-butyl levulinate by esterification of levulinic acid with 1-butene over ion-exchange resins. *Fuel Process. Technol.* **2021**, *220*, 106893. [[CrossRef](#)]
26. Bastos, R.R.C.; da Luz Corrêa, A.P.; da Luz, P.T.S.; da Rocha Filho, G.N.; Zamian, J.R.; da Conceição, L.R.V. Optimization of biodiesel production using sulfonated carbon-based catalyst from an amazon agro-industrial waste. *Energy Convers. Manag.* **2020**, *205*, 112457. [[CrossRef](#)]
27. Gaide, I.; Makareviciene, V.; Sendzikiene, E.; Gumbyte, M. Application of dolomite as solid base catalyst for transesterification of rapeseed oil with butanol. *Sustain. Energy Technol. Assess.* **2022**, *52*, 102278. [[CrossRef](#)]
28. Kirubakaran, M.; Selvan, V.A.M. Experimental investigation on the effects of micro eggshell and nano-eggshell catalysts on biodiesel optimization from waste chicken fat. *Bioresour. Technol. Rep.* **2021**, *14*, 100658. [[CrossRef](#)]
29. Ajala, E.O.; Ehinmowo, A.B.; Ajala, M.A.; Ohiro, O.A.; Aderibigbe, F.A.; Ajao, A.O. Optimisation of CaO–Al<sub>2</sub>O<sub>3</sub>–SiO<sub>2</sub>–CaSO<sub>4</sub>-based catalysts performance for methanolysis of waste lard for biodiesel production using response surface methodology and meta-heuristic algorithms. *Fuel Process. Technol.* **2022**, *226*, 107066. [[CrossRef](#)]
30. Balamurugan, S.; Gokul, C.; Dheen, S.A.T.; Eashwar, S.J.; Kumar, N.A. Application of grey relational analysis in biodiesel production from linseed oil using novel eggshell catalyst. *Mater. Today Proc.* **2021**, *45*, 1962. [[CrossRef](#)]
31. Novaes, C.G.; Yamaki, R.T.; de Paula, V.F.; Júnior, B.B.D.N.; Barreto, J.A.; Valasques, G.S.; Bezerra, M.A. Optimization of Analytical Methods Using Response Surface Methodology—Part I: Process Variables. *Rev. Virtual De Química* **2017**, *9*, 1184. [[CrossRef](#)]
32. Gonçalves, M.A.; Mares, E.K.L.; Zamian, J.R.; da Rocha Filho, G.N.; da Conceição, L.R.V. Statistical optimization of biodiesel production from waste cooking oil using magnetic acid heterogeneous catalyst MoO<sub>3</sub>/SrFe<sub>2</sub>O<sub>4</sub>. *Fuel* **2021**, *304*, 121463. [[CrossRef](#)]
33. de Brito, V.L.; Gonçalves, M.A.; Santos, H.C.L.D.; da Rocha Filho, G.N.; da Conceição, L.R.V. Biodiesel production from waste frying oil using molybdenum over niobia as heterogeneous acid catalyst: Process optimization and kinetics study. *Renew. Energy* **2023**, *215*, 118947. [[CrossRef](#)]
34. Pinto, B.F.; Garcia, M.A.S.; Costa, J.C.S.; de Moura, C.V.R.; de Abreu, W.C.; de Moura, E.M. Effect of calcination temperature on the application of molybdenum trioxide acid catalyst: Screening of substrates for biodiesel production. *Fuel* **2019**, *239*, 290. [[CrossRef](#)]
35. Dantas, J.; Leal, E.; Mapossa, A.B.; Pontes, J.R.M.; Freitas, N.L.; Fernandes, P.C.R.; Costa, A.C.F.M. Biodiesel production on bench scale from different sources of waste oils by using NiZn magnetic heterogeneous nanocatalyst. *Int. J. Energy Res.* **2021**, *45*, 10924. [[CrossRef](#)]
36. Hou, X.; Huang, J.; Liu, M.; Li, X.; Hu, Z.; Feng, Z.; Zhang, M.; Luo, J. Single-Crystal MoO<sub>3</sub> Micrometer and millimeter belts prepared from discarded molybdenum disilicide heating elements. *Sci. Rep.* **2018**, *8*, 1. [[CrossRef](#)] [[PubMed](#)]
37. Al-Alotaibi, A.L.; Altamimi, N.; Howsawi, E.; Elsayed, K.A.; Massoudi, I.; Ramadan, A.E. Synthesis and Characterization of MoO<sub>3</sub> for Photocatalytic Applications. *J. Inorg. Organomet. Polym. Mater.* **2021**, *31*, 2017. [[CrossRef](#)]
38. Sales, H.B.; Menezes, R.R.; Neves, G.A.; Souza, J.J.N.; Ferreira, J.M.; Chantelle, L.; de Oliveira, A.L.M.; Lira, H.D.L. Development of Sustainable Heterogeneous Catalysts for the Photocatalytic Treatment of Effluents. *Sustainability* **2020**, *12*, 7393. [[CrossRef](#)]
39. Joya, M.; Alfonso, J.; Moreno, L. Photoluminescence and Raman studies of α-MoO<sub>3</sub> doped with erbium and neodymium. *Curr. Sci.* **2019**, *116*, 1690. [[CrossRef](#)]
40. Moura, J.; Silveira, J.; da Silva Filho, J.; Filho, A.S.; Luz-Lima, C.; Freire, P. Temperature-induced phase transition in h-MoO<sub>3</sub>: Stability loss mechanism uncovered by Raman spectroscopy and DFT calculations. *Vib. Spectrosc.* **2018**, *98*, 98. [[CrossRef](#)]
41. Zhang, C.; Zheng, L.; Zhang, Z.; Dai, R.; Wang, Z.; Zhang, J.; Ding, Z. Raman studies of hexagonal MoO<sub>3</sub> at high pressure. *Phys. Status Solidi* **2011**, *248*, 1119. [[CrossRef](#)]
42. Chaves-Lopez, C.; Nguyen, H.N.; Oliveira, R.C.; Nadres, E.T.; Paparella, A.; Rodrigues, D.F. A morphological, enzymatic and metabolic approach to elucidate apoptotic-like cell death in fungi exposed to h- and alpha-molybdenum trioxide nanoparticles. *Nanoscale* **2018**, *10*, 20702. [[CrossRef](#)] [[PubMed](#)]
43. Shahsank, M.; Naik, H.S.B.; Sumedha, H.N.; Nagaraju, G. Implementing an in-situ carbon formation of MoO<sub>3</sub> nanoparticles for high performance lithium-ion battery. *Ceram. Int.* **2021**, *47*, 10261. [[CrossRef](#)]
44. Prakash, N.G.; Dhananjaya, M.; Narayana, A.L.; Shaik, D.P.M.D.; Rosaiah, P.; Hussain, O.M. High Performance One Dimensional α-MoO<sub>3</sub> Nanorods for Supercapacitor Applications. *Ceram. Int.* **2018**, *44*, 9967. [[CrossRef](#)]
45. Rammal, M.B.; Omanovic, S. Synthesis and characterization of NiO, MoO<sub>3</sub>, and NiMoO<sub>4</sub> nanostructures through a green, facile method and their potential use as electrocatalysts for water splitting. *Mater. Chem. Phys.* **2020**, *255*, 123570. [[CrossRef](#)]
46. Paula, H.M.D.; Fernandes, C.E. Otimização do tratamento de água cinza a partir do uso combinado de coagulantes químicos. *Eng. Sanit. E Ambient.* **2018**, *23*, 951. [[CrossRef](#)]

47. Jain, S.; Adiga, K.; Verneker, V.P. A new approach to thermochemical calculations of condensed fuel-oxidizer mixtures. *Combust. Flame* **1981**, *40*, 71. [[CrossRef](#)]
48. Silva, A.L.D.; Costa, A.C.F.D.M.; Farias, A.F.F.; Araujo, R.G. Dispositivo De Patente: Br 10 2021 018179 6—Síntese Por Reação De Combustão Do MoO<sub>3</sub> Para Uso Como Catalisador Heterogêneo. *Rev. De Propr. Ind. RPI RPI* **2021**, *2725*, 36.
49. Costa, A.; Kiminami, R. Dispositivo para produção de nanomateriais cerâmicos em larga escala por reação de combustão e processo contínuo de produção dos nanomateriais BR 10 2012 002180 3. *Rev. De Propr. Ind. RPI* **2012**, *25*, 002181.
50. Amenaghawon, A.N.; Evbarunegbe, N.I.; Obahiagbon, K. Optimum biodiesel production from waste vegetable oil using functionalized cow horn catalyst: A comparative evaluation of some expert systems. *Clean. Eng. Technol.* **2021**, *4*, 100184. [[CrossRef](#)]
51. Patil, S.A.; Arakerimath, D.R.R. Biodiesel Production Optimization using Heterogeneous Catalyst (Al<sub>2</sub>O<sub>3</sub>) in Karanja oil by Taguchi Method. *Int. J. Recent Technol. Eng. (IJRTE)* **2019**, *8*, 5555. [[CrossRef](#)]
52. Klug, H.P.; Alexander, L.E. *X-ray Diffraction Procedures: For Polycrystalline and Amorphous Materials*; Wiley: Hoboken, NJ, USA, 1974.

**Disclaimer/Publisher's Note:** The statements, opinions and data contained in all publications are solely those of the individual author(s) and contributor(s) and not of MDPI and/or the editor(s). MDPI and/or the editor(s) disclaim responsibility for any injury to people or property resulting from any ideas, methods, instructions or products referred to in the content.